Hearing Research xxx (xxxx) xxx

Contents lists available at ScienceDirect

Hearing Research

journal homepage: www.elsevier.com/locate/heares

Research Paper

In vivo whole-cell recordings of stimulus-specific adaptation in the inferior colliculus

Catalina Valdés-Baizabal [a, b, 1, 2], Lorena Casado-Román [a, b, 2], Edward L. Bartlett [c, d], Manuel S. Malmierca [a, b, e, *]

[a] Cognitive and Auditory Neuroscience Laboratory, Institute of Neuroscience of Castilla y León, University of Salamanca, 37007, Salamanca, Spain
[b] The Salamanca Institute for Biomedical Research (IBSAL), 37007, Salamanca, Spain
[c] Department of Biological Sciences, Purdue University, West Lafayette, IN, 47907, USA
[d] Weldon School of Biomedical Engineering, Purdue University, West Lafayette, IN, 47907, USA
[e] Department of Cell Biology and Pathology, Faculty of Medicine, Campus Miguel de Unamuno, University of Salamanca, 37007, Salamanca, Spain

ARTICLE INFO

Article history:
Received 10 January 2020
Received in revised form
17 April 2020
Accepted 18 April 2020
Available online xxx

Keywords:
Stimulus-specific adaptation
Inferior colliculus
In vivo whole-cell
Current-clamp
Intrinsic properties
Subthreshold responses

ABSTRACT

The inferior colliculus is an auditory structure where inputs from multiple lower centers converge, allowing the emergence of complex coding properties of auditory information such as stimulus-specific adaptation. Stimulus-specific adaptation is the adaptation of neuronal responses to a specific repeated stimulus, which does not entirely generalize to other new stimuli. This phenomenon provides a mechanism to emphasize saliency and potentially informative sensory inputs. Stimulus-specific adaptation has been traditionally studied analyzing the somatic spiking output. However, studies that correlate within the same inferior colliculus neurons their intrinsic properties, subthreshold responses and the level of acoustic stimulus-specific adaptation are still pending. For this, we recorded *in vivo* whole-cell patch-clamp neurons in the mouse inferior colliculus while stimulating with current injections or the classic auditory oddball paradigm.

Our data based on cases of ten neuron, suggest that although passive properties were similar, intrinsic properties differed between adapting and non-adapting neurons. Non-adapting neurons showed a sustained-regular firing pattern that corresponded to central nucleus neurons and adapting neurons at the inferior colliculus cortices showed variable firing patterns. Our current results suggest that synaptic stimulus-specific adaptation was variable and could not be used to predict the presence of spiking stimulus-specific adaptation. We also observed a small trend towards hyperpolarized membrane potentials in adapting neurons and increased synaptic inhibition with consecutive stimulus repetitions in all neurons. This finding indicates a more simple type of adaptation, potentially related to potassium conductances. Hence, these data represent a modest first step in the intracellular study of stimulus-specific adaptation in inferior colliculus neurons *in vivo* that will need to be expanded with pharmacological manipulations to disentangle specific ionic channels participation.

1. Introduction

The inferior colliculus (IC) is a midbrain structure that integrates auditory inputs from ascending and descending pathways in the auditory system. The IC is the first auditory structure where inputs from lower auditory centers, including the cochlear nucleus, superior olivary complex and lateral lemniscus, converge and send information to the thalamus (Ito and Malmierca, 2018; Malmierca, 2015). The IC is divided into the central nucleus (CNIC) within the lemniscal pathway and the surrounding cortices (dorsal, lateral and rostral) belonging to the nonlemniscal pathway (Ito and Malmierca, 2018; Loftus et al., 2008; Malmierca et al., 2011, 1993). Both pathways present different connection patterns and neuronal type organization (Ito and Malmierca, 2018; Malmierca, 2015). The multiple patterns of afferent convergence allow the emergence of complex coding properties of auditory information such as

* Corresponding author. Cognitive and Auditory Neuroscience Laboratory, Institute of Neuroscience of Castilla y León, University of Salamanca, 37007, Salamanca, Spain.
E-mail address: msm@usal.es (M.S. Malmierca).
[1] Present address: Laboratory of Cellular Neurobiology, Department of Basic Medical Sciences, Section of Medicine, Faculty of Health Sciences, University of La Laguna, 38200 Sta. Cruz de Tenerife, Spain.
[2] These authors contributed equally.

https://doi.org/10.1016/j.heares.2020.107978

List of abbreviations

AP	action potential
CNIC	central nucleus of the inferior colliculus
CSI	common stimulus-specific adaptation index
DCIC	dorsal cortex of the inferior colliculus
DEV	deviant tones
EPSP	excitatory postsynaptic potentials
EPSP-CSI	excitatory postsynaptic potential common stimulus-specific adaptation index
FRA	frequency response area
IC	inferior colliculus
IPSP	inhibitory postsynaptic potentials
IPSP-CSI	inhibitory postsynaptic potential common stimulus-specific adaptation index
last-STD	last-standard tones before a deviant events
LCIC	lateral cortex of the inferior colliculus
next-STD	next-standard tones after a deviant events
n.s.	non-statistically significant difference
PSPs	postsynaptic potentials
PSTH	peristimulus time histogram
SEM	standard error of the mean
SSA	stimulus-specific adaptation
STD	all standard tones
Vm	membrane potential

stimulus-specific adaptation (SSA; Ayala and Malmierca, 2013; Duque et al., 2012; Lumani and Zhang, 2010; Malmierca et al., 2009a,b; Pérez-González et al., 2005; Zhao et al., 2011). SSA is the adaptation of neuronal responses to a specific repeated stimulus, which does not entirely generalize to other different stimuli (Movshon and Lennie, 1979; Ulanovsky et al., 2003). Comparing the responses to a highly repeated standard sound and a rare deviant sound in an oddball paradigm, strong SSA occurs when the responses to the deviant sound are much larger than those for the standard events. This phenomenon provides a mechanism to emphasize salient and potentially informative sensory inputs, which may serve multiple functions such as deviance detection, auditory memory and recognition of acoustic objects (Ayala and Malmierca, 2013).

The IC is also the first region where SSA is evident in the mammalian auditory pathway (Ayala et al., 2013; Duque et al., 2018; Pérez-González et al., 2005), but the cellular mechanisms that govern and contribute to SSA generation are elusive. SSA is typically measured for the somatic spiking output, which results from the interaction between membrane properties, especially the spiking threshold, synaptic inputs, and the tuning characteristics of the inputs. SSA is not evenly distributed within the IC. Neurons in the cortices exhibit strong SSA, while neurons in the CNIC typically have much weaker or lack SSA (Ayala and Malmierca, 2013; Duque et al., 2012; Malmierca et al., 2009a). The inputs associated with the neurons of both the cortices and the CNIC of the IC have been characterized (Ayala et al., 2016). There is a diversity of IC membrane properties, but they broadly fit into onset, accommodating and sustained classes (Geis and Borst, 2013; Kuwada et al., 1997; Ma et al., 2002; Peruzzi et al., 2000; Rabang et al., 2012; Sun et al., 2006; Tan et al., 2007; Wu et al., 2004). Post-synaptic responses to randomly presented pure tones have also been characterized in the IC and are similar to suprathreshold activity. The dorsal cortex of the IC (Geis and Borst, 2013; Geis et al., 2011) shows broad and complex frequency response areas, whereas the CNIC displays sharp tuning, clear tonotopic organization and shorter-latency responses (Geis and Borst, 2009). However, to fully understand SSA, the intrinsic biophysical excitability of a neuron should be integrated with its synaptic physiology, which shapes dynamic information processing (Malinowski et al., 2019). To date, studies that determine within the same neurons their intrinsic neuronal properties, subthreshold responses and their level of acoustic SSA are still pending in the IC *in vivo*. It is important to study these interactions because they might help to understand why non-lemniscal or cortical IC regions exhibit stronger SSA. We propose the hypothesis that adapting (SSA) neurons and non-adapting (no SSA) neurons in the IC differ in their intrinsic neuronal properties and/or subthreshold responses. Thus, the present study aims at determining the possible correlation between the intrinsic neuronal properties (i.e., firing patterns in response to current injections), passive membrane properties, subthreshold responses with their adaptation properties of the IC neurons. These correlations can only be addressed with intracellular recordings, which allow measuring subthreshold postsynaptic responses and responses to current injection. Likewise, we can correlate the level of adaptation from the synaptic input with that of the spiking output response.

2. Methods

2.1. Surgical procedure

Experiments were performed in 10 adult mice (CBA/J; body weights: 22–36 g; ~2–3 months old). All experimental procedures were carried out at the University of Salamanca using methods conforming to the standards of the European Union Directive 2010/63/EU and the Spanish Royal Decree 53/2013 for the use of animals in research and approved by the Bioethics Committee of the University of Salamanca.

Surgical anesthesia was induced with an intraperitoneal injection of ketamine-acepromazine-dexmedetomidine (75, 1 and 1 mg/kg, respectively), which is an optimum cocktail recommended for long surgical or experimental procedures (Flecknell, 2009). A stable anesthetic level was maintained with supplementary doses of ¼ of the induction dose when pedal withdrawal reflexes were present. Body temperature was maintained at 37 °C with a homeothermic blanket system (Cibertec). Glucosaline solution was administered subcutaneously to prevent dehydration (~0.25 ml). The animal was placed in a stereotaxic frame and the skull was surgically exposed. A head-post was cemented with dental acrylic to immobilize the head during recordings. To expose the IC, a craniotomy of ~2 mm in diameter was performed and the dura was removed.

2.2. Whole-cell patch-clamp electrophysiological recordings

We obtained *in vivo* whole-cell recordings with a non-visually guided or blind approach (Margrie et al., 2002). We pulled borosilicate glass pipettes with filament (1.5 mm outer diameter, 0.315 mm wall thickness; World Precision Instruments) to have a resistance of 8 ± 1 MΩ (1–2 μm tip, P-1000 puller from Sutter Instruments). Pipettes were filled with intracellular solution containing (in mM): K-gluconate 125, KCl 20, EGTA 0.5, HEPES 10, Na_2-phosphocreatine 10, Mg-ATP 4 and Na_2-GTP 0.3 (pH 7.2 with KOH and osmolarity between 290 and 300 mOsm).

To keep the brain surface moist and reduce the cerebral pulsations during recordings, the craniotomy was covered with a thin

Please cite this article as: Valdés-Baizabal, C et al., *In vivo* whole-cell recordings of stimulus-specific adaptation in the inferior colliculus, Hearing Research, https://doi.org/10.1016/j.heares.2020.107978

layer of 2% agarose in ringer solution ([in mM]: NaCl 135, KCl 5.4, $MgCl_2$ 1, $CaCl_2$ 1.8 and HEPES 5 [pH 7.2 with NaOH]). The pipette was introduced into the mouse IC with penetration angles from 10° to 30° and advanced with a micromanipulator (Scientifica). The initial pipette pressure was ~200 mmHg and the pressure was reduced to ~30 mmHg when approaching a cell. The recorded neurons were located at penetration depths ranging from 81 to 600 μm.

2.3. Current injection protocol

We recorded membrane potential (Vm) variations in current-clamp mode during sound stimulation (see section 2.4. below) and during the injection of square current pulse series from −400 pA to 200 pA above the firing threshold, with 100 pA steps and 300 ms pulse lengths. Signals were sampled at 10 kHz, low-pass filtered at 10 kHz and amplified with a MultiClamp 700B Amplifier (Molecular Devices). Command pulse generation and data acquisition were performed with the Axon™ Digidata® 1550A Low-Noise Data Acquisition System *plus* HumSilencer™ Adaptive Noise Cancellation (Molecular devices) controlled by pCLAMP 10.5.0.9 software (Molecular Devices). Thereby, we determined the action potential (AP) threshold and the discharge pattern, the interspike interval, the depolarizing sag generated by hyperpolarizing current pulses (Almanza et al., 2012) and the number of rebound APs of each neuron. We estimated the AP threshold as the value of the current injection at which each neuron discharged AP(s). The amplitude of the depolarizing sag was calculated as the ratio between the voltage at the maximum peak of the most hyperpolarizing pulse (−400 pA) and the voltage of the stable state at the end of the most hyperpolarizing pulse. We assessed the time constant tau adjusting the most hyperpolarizing pulse to a single-exponential function (correlation coefficient > 0.99).

Based on the discharge pattern, we classified neurons as sustained, accommodating, accelerating or burst onset cells. We used the term "accommodating" instead of adapting used by others (Sivaramakrishnan and Oliver, 2001) to avoid confusion with the SSA property treated in the context of this paper. Firing patterns were determined following the work of Sivaramakrishnan and Oliver (2001) and Tan et al. (2007). Briefly, firing patterns were classified at 100 pA above the smallest suprathreshold current injection. Burst-onset cells fire a cluster of two or more APs at the depolarization onset. Accelerating neurons increase their firing rate along with the depolarizing current injection. Accommodating cells present precisely the opposite profile with decreasing firing rates. Sustained neurons fire with a nearly constant interspike interval during the depolarizing pulse. Cells with rebound spikes present them after hyperpolarization pulses. The interspike interval was measured as the time between spikes, while the instantaneous frequency was calculated (automatically by clampfit) by converting each interspike interval into a frequency, and then, averaging these frequencies together.

Membrane potentials were corrected offline for an estimated −11 mV junction potential (Neher, 1992). Data of passive properties (capacitance and membrane resistance) were acquired online and verified offline. We performed analyses offline using Clampfit in the pClamp 10.5.0.9 bundle (Molecular Devices) and SigmaPlot® 11.0 software. To ensure reliable data quality, neurons were discarded from the study when membrane voltage depolarized beyond −44 mV and did not recover the initial membrane potential; auditory or current injection protocols were incomplete; cells did not show APs nor PSPs after sound stimulation with pure tones, following previous work (Tan et al., 2007).

2.4. Sound stimulation and data analyses

We performed experiments in a sound-attenuating chamber. Stimuli were delivered through an electrostatic open-field speaker (TDT-EC1, Tucker-Davis Technologies [TDT]) placed close to the contralateral ear. Stimulus generation and online data visualization were controlled with the RZ6 Multi I/O Processor (TDT), pCLAMP 10.5 (Molecular Devices) and custom software programmed with OpenEx Suite (TDT) and MATLAB (Mathworks). We calibrated the sound system *in situ* using a ¼ inch condenser microphone (model 4136, Brüel & Kjær) and a dynamic signal analyzer (Photon+, Brüel & Kjær). The maximum sound system output was flat between 0.5 and 4.5 kHz (77.11 ± 0.38 dB SPL) and between 5 and 40 kHz (~85 ± 5 dB SPL). The second and third signal harmonics were at least 40 dB lower than the fundamental frequency at the highest output level (Malmierca et al., 2009a).

The monaural frequency response area (FRA; i.e., the combination of frequencies and intensities capable of evoking a response), was then obtained using a randomized presentation of pure tones. Pure tones lasted 75 ms (5 ms rise/fall ramps) and were separated by an onset-to-onset interval of 250 ms. Frequency and intensity of the stimulus varied randomly (0–70 dB SPL in 10 dB steps and 0.1–40 kHz in 25 frequency steps to cover approximately 2–3 octaves above and below the best frequency (i.e., the frequency with the lowest intensity threshold; Hernández et al., 2005).

To study the level of SSA per neuron, we used the classic oddball paradigm following previous studies in our laboratory (Ayala et al., 2013; Ayala and Malmierca, 2018, 2015; Duque et al., 2016, 2012; Malmierca et al., 2019, 2009a; Pérez-González et al., 2012, 2005; Valdés-Baizabal et al., 2017). We selected two frequencies from the FRA of each cell to generate the oddball paradigm. The two frequencies elicited comparable firing rates in the FRA. They were around the characteristic frequency, which is the tone frequency that produces a response at the lowest stimulus level. We presented trains of 400 stimuli at a specific repetition rate (4 Hz) and a level of 10–40 dB above the response threshold. For each neuron, sequences consisted of pure tones of two different frequencies with a ~0.28-octave frequency separation, which were selected within its excitatory FRA. One frequency (f_1) was presented as standard (i.e., a higher probability of occurrence within the sequence, $p = 0.9$); interspersed pseudo-randomly with the second frequency (f_2) presented as deviant (i.e., low probability within the sequence, $p = 0.1$). Sequences began with a minimum of 10 repetitions of standard stimuli, and a minimum of 3 standard tones separated deviant events. After obtaining one data set, the relative probabilities of the two stimuli were reversed, with f_2 as the standard and f_1 as the deviant. Pure tones lasted 75 or 30 ms (5 ms rise/fall ramps) and were separated by an onset-to-onset interval of 250 or 300 ms, respectively.

We analyzed and illustrated data with Clampfit 10.5 (Molecular Devices), SigmaPlot® 11.0 software and custom-written MATLAB scripts. We computed spike counts and peristimulus time histograms (PSTH) with the AP times in response to every stimulus and tested condition, both in the FRA and oddball paradigm. To visualize responses to oddball paradigms, PSTHs were computed with the mean firing rate of the 40 trials of deviant events, 360 trials of standard events and the 40 trials of the standard events preceding the deviant tones (i.e., the tones with the strongest adaptation; named from now onwards as last-standard stimuli). To calculate the adaptation properties of each neuron, we computed the Common SSA Index (CSI); we measured the total firing rate for each condition as the average spike count within the 40 trials of deviant tones and the 40 trials of the last-standard events. The CSI determines the level of SSA for both frequencies of the oddball paradigm at each condition and classifies neurons as adapting

Please cite this article as: Valdés-Baizabal, C et al., *In vivo* whole-cell recordings of stimulus-specific adaptation in the inferior colliculus, Hearing Research, https://doi.org/10.1016/j.heares.2020.107978

(CSI > 0.25) and non-adapting (CSI ≤ 0.25) as previous studies (Antunes et al., 2010; Ayala et al., 2015, 2013; Duque et al., 2012; Malmierca et al., 2009a). The CSI was calculated with the spike counts for each neuron and the two frequencies of the oddball paradigm (f_1 and f_2):

$$CSI = \frac{\sum Deviant(f_i) - \sum Standard(f_i)}{\sum Deviant(f_i) + \sum Standard(f_i)}; i = 1, 2$$

where Deviant (f_i), Standard (f_i) are spike counts in response to frequency f_i presented as a deviant and standard event, respectively. CSI reflects to what extent the response of standard stimuli was suppressed or adapted. The index ranges between −1 and 1, being positive if the response to the deviant stimulus was greater than the response to the standard stimulus. Thereby, we classified neurons as classically done with CSI values derived from APs measurements. Similarly, we also computed CSIs with postsynaptic potentials (PSPs) to determine whether SSA is reflected in membrane potentials at the subthreshold level. Hence, we can correlate the adaptation-level of the final firing output response with the synaptic input of each cell. Accordingly, we tested the changes in the membrane voltage around stimulus presentation. For this purpose, we removed spiking activity from the voltage trace by replacing the spike with a linear interpolation between the start to the end of the spike and measured the mean membrane potential and areas of excitatory PSPs (EPSPs) and inhibitory PSPs (IPSPs) in analysis windows. We defined the baseline window 75 ms before each stimulus onset and the analysis window of 0–150 ms after stimulus onset for both onset-to-onset intervals and tone durations. Excitatory areas were measured above the mean membrane potential of the baseline plus 1 standard deviation, whereas inhibitory areas were measured below the mean membrane potential of the baseline minus 1 standard deviation. We then computed the CSI values for the excitatory (EPSP-CSI) and the inhibitory (IPSP–CSI) areas in separate with the same CSI equation. This time instead of using the number of APs, we computed the response to standard events as the sum of the area measurements of the 40 stimulus repetitions of the last-standard stimuli and the response to deviant events the sum of the 40 deviant events similarly to previous work in the auditory cortex (Chen et al., 2015). With the measurement of excitatory and inhibitory PSPs areas, we could calculate the CSI with the previous equation. Additionally, to explore the time course of EPSPs and IPSPs, we analyzed the onset latencies of the largest excitatory and inhibitory areas as the first time point of each stimulus repetition. Mean latencies were calculated separately for excitation and inhibition per neuron and stimulus condition.

In the same analysis window from 0 to 150 ms after stimulus onset, we also analyzed mean evoked responses of the excitatory areas, inhibitory areas and the membrane potential according to each stimulus condition: deviant tones, all standard tones, last-standard tones, next-standard tones after deviant events and the standard tones separated according to the number of consecutive standard tones previously presented. To be considered for the analysis, at least a minimum of 20 repetitions of each condition within a stimulation sequence needed to occur. We normalized each response variable within each neuron with the greatest response of all stimuli presented as part of the two oddball sequences. We then determined the correlation between the number of consecutive standard repetitions and the mean values of the normalized mean membrane potential responses, excitatory or inhibitory areas in the entire population with *Pearson correlation analyses.*

2.5. Statistical testing

Data are denoted as means ± standard error of the mean (SEM). To statistically compare the analyzed parameters between neurons grouped according to their CSI levels (adapting neurons, non-adapting neurons and non-spiking neurons with sound-evoked PSPs [i.e., neurons without tone-evoked APs but with tone-evoked PSPs]), we calculated One-Way ANOVA as denoted in Results. When comparisons were statistically different, samples were tested with a Holm-Sidak method. The significance level was set at $\alpha = 0.05$.

2.6. Histology

One cell was biocytin-labeled for histological identification. We used an intracellular solution containing 1% biocytin, which was ejected during the current injection protocol. Five min after injection, the patch pipette was retracted slowly. The animal was transcardially perfused with 4% paraformaldehyde in phosphate-buffered saline and cryoprotected in 30% sucrose. 40 μm sections were cut in the coronal plane with a freezing microtome. The location of biocytin-filled neurons was visualized with an avidin-biotinylated horseradish peroxidase complex with minor modifications to that described by Brandt and Apkarian (1992); Veenman et al. (1992).

3. Results

We recorded *in vivo* whole-cell patch-clamp neurons in the mouse IC while using two types of stimulation: current injection and auditory stimulation. We successfully recorded 10 neurons with an adequate average resting membrane potential of −57.8 ± 3.06 mV, average membrane capacitance of 9 ± 2 pF and average membrane resistance of 510 ± 63.5 MΩ. The access resistance was 14.1 ± 3.7 MΩ. Fig. 1 shows one of these neurons that was histologically labeled in the dorsal cortex of the IC with a pipette solution containing 1% biocytin as control of whole-cell patch-clamp. For all neurons, we recorded their FRA and selected the tones comprising the oddball paradigms (tones of a range of frequencies [2.9–31 kHz; mean 14.95 ± 1.10 kHz] and intensities [20.2–57.2 dB SPL; mean 36.19 ± 2.56 dB SPL].

3.1. Classification of the inferior colliculus neurons by their adaptation levels

To quantify the degree of SSA using the oddball paradigm, we computed the CSI with the spiking activity. This analysis allowed us to classify 4 neurons as adapting neurons (CSI > 0.25; mean CSI = 0.79 ± 0.09), 3 as non-adapting neurons (CSI ≤ 0.25; mean CSI = −0.05 ± 0.04) and 3 additional neurons as non-spiking with sound-evoked PSPs (see CSI values in Table 1; Fig. 2 for examples of membrane potential traces). These 3 non-spiking neurons did not fire APs but responded with PSPs to pure tones. Also, the non-spiking neurons with sound-evoked PSPs discharged APs during the injection of current pulses. The adapting neurons exhibited non-V-shaped FRAs without a clear best frequency characteristic of the cortices of the IC (Neuron 3 on Fig. 3A), whereas the non-adapting neurons showed V-shaped FRAs with characteristic frequencies typical of the CNIC (Neuron 5 on Fig. 3A). CSI values accurately represented the adaptation properties of a neuron. CSI levels within the same neurons classified equally across the various stimulation conditions (frequencies, tone duration, intensity and onset-to-onset interval; see Table 1 for specificities) and thus, data were merged for subsequent comparisons according to their CSI. All neuronal groups had two stimulus durations and onset-to-onset

Please cite this article as: Valdés-Baizabal, C et al., *In vivo* whole-cell recordings of stimulus-specific adaptation in the inferior colliculus, Hearing Research, https://doi.org/10.1016/j.heares.2020.107978

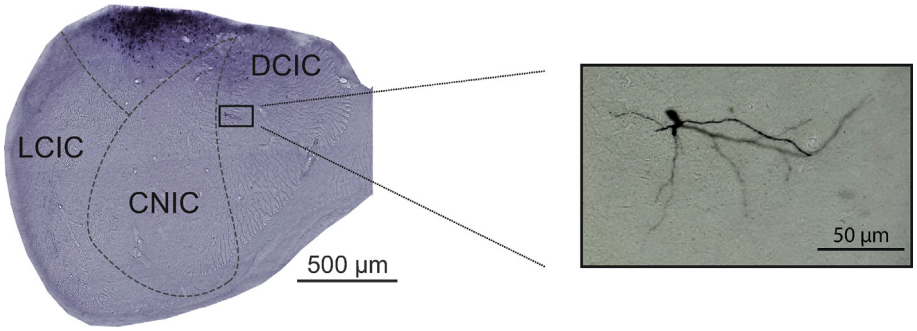

Fig. 1. Anatomical location of neurophysiological recordings. Histological coronal section (40 µm thickness) of one of the non-spiking neurons with sound-evoked PSPs (neuron 10) that was biotinylated (1% of the intracellular solution and a reduced K-gluconate concentration to 115 mM) together with the location of fields of the IC on a mouse brain atlas (bregma −5.3 mm). At higher magnification, this neuron shows a partially labeled dendritic tree extending parallel to the cortical surface. This neuron was localized in the dorsal cortex of the IC. The dark region above the cell is due to the pipette's positive pressure that leaks out biocytin while approaching the cell. The location of biocytin-filled neurons was visualized with an avidin-biotinylated horseradish peroxidase complex with minor modifications to that described by Brandt and Apkarian (1992); Veenman et al. (1992). LCIC: lateral cortex of the inferior colliculus, DCIC: dorsal cortex of the inferior colliculus, CNIC: central nucleus of the inferior colliculus.

Table 1
Common stimulus-specific adaptation indices computed with the absolute number of evoked action potentials (CSI), the sum of excitatory response areas of the membrane voltage (EPSP-CSI) and the sum of inhibitory response areas of the membrane voltage (IPSP−CSI) for all the recorded stimulus conditions.

	Neuron #	Onset-to-onset interval (ms)	Tone duration (ms)	Frequencies (KHz)	Intensity (dB SPL)	CSI	EPSP-CSI	IPSP-CSI
Adapting neurons	1	300	30	11.6 & 14.2	32.5	0.76	0.03	−0.03
		300	30	10.6 & 15.3	32.5	0.95	0.06	−0.19
		300	30	16.2 & 19.8	39.5	0.69	0.14	−0.25
		300	30	14.4 & 20.8	39.5	1	0.45	−0.42
	2	250	75	8.3 & 10.1	43.2	0.86	0.00	0.02
	3	250	75	16.2 & 19.8	30.2	0.96	0.07	−0.09
	4	250	75	13.0 & 16.0	47.2	0.28	−0.06	0.07
Non-adapting neurons	5	250	75	9.0 & 11.0	39.5	−0.05	0.01	−0.01
		250	75	9.5 & 10.5	39.5	−0.09	0.00	−0.01
		300	30	9.6 & 11.7	25.5	−0.14	0.00	−0.10
		300	30	10.0 & 11.2	25.5	−0.11	0.00	0.02
		300	30	9.5 & 10.5	39.5	−0.05	0.00	0.02
	6	300	30	12.7 & 15.5	49.5	−0.1	−0.00	0.05
	7	250	75	18 & 22	20.4	0.17	0.03	0.07
Non-spiking neurons with sound-evoked PSPs	8	250	75	25 & 31	48.5	–	−0.00	−1
		300	30	21.0 & 26.0	21.5	–	0.06	−0.25
	9	250	75	2.9 & 3.5	57.2	–	0.15	−0.17
	10	250	75	23.3 & 28.4	20.2	–	0.04	−0.08

intervals and frequencies and intensities were comparable across groups (One-Way ANOVA, frequencies [$p = 0.170$], intensities [$p = 0.589$]).

Adaptation is a property that has been traditionally studied analyzing APs. However, it is currently unknown whether the neuronal subthreshold responses differ between IC neurons adapting their spiking response to those non-adapting neurons. Given that cochlear nucleus neurons do not exhibit adaptation (Ayala et al., 2013; Duque et al., 2018), then the question arises as to whether or not spiking adaptation results from PSP adaptation in the IC. To correlate the PSPs with the classic CSIs of spiking activity, we computed the CSI for inhibitory and excitatory areas separately to explore what influence excitation and inhibition have under the deviant and standard conditions (Fig. 3C, EPSP-CSI and IPSP-CSI in Table 1). EPSP-CSI and IPSP-CSI were around 0, meaning that deviant and standard tones evoked a comparable amount of excitation and inhibition. Interestingly, a non-spiking neuron with sound-evoked PSPs showed higher inhibitory responses to the last-standard tones than deviant events (IPSP−CSI = −1). Overall, this data demonstrated no general differences in the excitatory or inhibitory synaptic inputs that each neuron receives regardless of its oddball adaptation profile. This finding supports the notion that there is a synaptic signal arrival in the form of PSPs after auditory stimulation regardless of the SSA properties of the APs.

To explore the time course of EPSPs and IPSPs, we further analyzed the mean onset latencies of the largest excitatory and inhibitory areas in deviant and last-standard events. Latencies of EPSPs for deviant and standard tones separately and all stimuli together across groups were comparable (Table 2; One-Way ANOVA, deviant tones [$p = 0.558$], standard tones [$p = 0.327$] and all stimuli [$p = 0.221$]). By contrast, inhibition was significantly faster in the non-adapting neurons than the adapting neurons after standard tones but not after deviant stimuli (One-Way ANOVA, standard events [$p = 0.035$] and deviant tones [$p = 0.05$]).

3.2. Comparisons of membrane potential responses between stimulus conditions

We grouped normalized responses within neurons of evoked responses measured according to stimulus condition. Evoked responses were computed as mean membrane potentials, as well as excitatory and inhibitory areas after stimulus presentation. The stimulus conditions were analyzed as deviant tones, all standard tones, last-standard tones, next-standard tones and the standard tones separated according to the number of consecutive standard tones previously presented (i.e., including up to 9 standard

Please cite this article as: Valdés-Baizabal, C et al., *In vivo* whole-cell recordings of stimulus-specific adaptation in the inferior colliculus, Hearing Research, https://doi.org/10.1016/j.heares.2020.107978

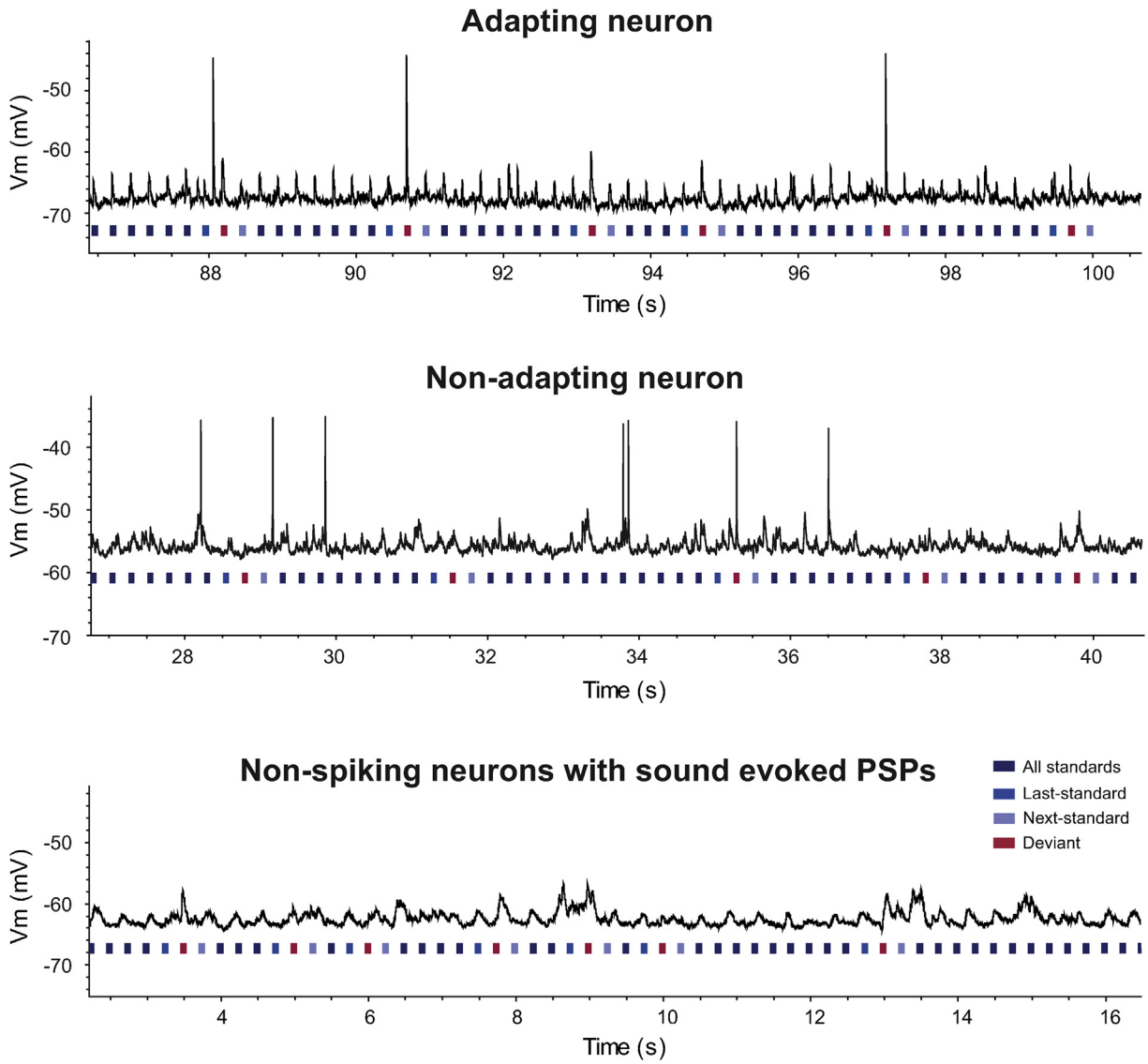

Fig. 2. Examples of membrane voltage traces of an adapting neuron (neuron 2), non-adapting neuron (neuron 7) and a non-spiking neuron with sound-evoked PSPs (neuron 9) classified based on their CSI levels of spiking activity. Horizontal red (deviant tones) and blue (standard tones denoting in separate the last- and next-standard events respect to deviant tones) bars indicate the epoch of sound stimulation. Action potentials and postsynaptic potentials were classified as deviant or standard stimuli accordingly from stimulus onset. Seconds denote time elapsed from the beginning of the stimulation sequence. Pure tones lasted 75 ms with an onset-to-onset interval of 250 ms.

stimulus repetitions). Comparisons among all these conditions of the mean membrane voltage and excitatory areas did not show any significant differences across groups of neurons (One-Way ANOVA with Repeated-Measures; $p > 0.05$ for all). However, inhibitory areas of deviant and next-standard tones were different between non-adapting and non-spiking neurons with sound-evoked PSPs (One-Way ANOVA with Repeated-Measures; $p < 0.05$). Interestingly, the 7th standard repetition demonstrated larger normalized IPSPs for the non-adapting neurons than the adapting cells (0.84 and 0.63, respectively $p = 0.019$). Next, we explored whether differences were within groups of neurons separately. Mean membrane potentials, excitatory and inhibitory areas for all stimulus conditions were similar within adapting neurons, non-adapting neurons and non-spiking neurons with sound-evoked PSPs (One-Way ANOVA; $p > 0.05$). Only adapting neurons showed a significantly more depolarized mean Vm of deviant events than all the other types of standard events ($p < 0.001$).

3.2.1. Data trends in the sequence of consecutive standard stimuli

We explored the membrane potential across the consecutive presentation of standard tones to find a possible link between the number of sound repetitions and the neuron's membrane potential. We performed *Pearson correlation analyses* between the number of consecutive standard repetitions and the mean values of the normalized mean Vm, excitatory or inhibitory areas in the entire population to determine a possible correlation. Results showed a significant relationship between the membrane potential from the 1st to the 6th consecutive standard presentation; mean membrane voltage tended to hyperpolarize in the group of the adapting neurons and slightly depolarized in the non-adapting neurons (adapting neurons, Pearson correlation coefficient $= -0.84$, $p = 0.04$; non-adapting neurons, Pearson correlation coefficient $= 0.57$, $p = 0.24$; non-spiking neurons with sound-evoked PSPs, Pearson correlation coefficient $= 0.03$, $p = 0.95$; population, Pearson correlation coefficient $= -0.24$, $p = 0.64$; see

Please cite this article as: Valdés-Baizabal, C et al., *In vivo* whole-cell recordings of stimulus-specific adaptation in the inferior colliculus, Hearing Research, https://doi.org/10.1016/j.heares.2020.107978

Fig. 4), whereas inhibition rose with an increasing number of consecutively presented standard tones at the population level (Pearson correlation coefficient = 0.69, p = 0.13) with only small trends within individual groups (adapting neurons, Pearson correlation coefficient = 0.16, p = 0.76; non-adapting neurons, Pearson correlation coefficient = 0.10, p = 0.85; non-spiking neurons with sound-evoked PSPs, Pearson correlation coefficient = 0.34, p = 0.51; see Fig. 4). By contrast, no strong correlation between excitatory areas and the number of consecutive standard tones was found (adapting neurons, Pearson correlation coefficient = 0.61, p = 0.20; non-adapting neurons, Pearson correlation coefficient −0.10, p = 0.85; non-spiking neurons with sound-evoked PSPs, Pearson correlation coefficient = 0.49, p = 0.32; population, Pearson correlation coefficient = 0.15, p = 0.77; Fig. 4).

We also analyzed the response mean membrane potential, inhibitory and excitatory areas to standard tones depending on the number of consecutive presentations for each neuron in separate (One-Way ANOVA and post hoc pairwise multiple comparisons with Holm-Sidak method; Table 3). Most significant differences were found in the groups of adapting neurons and non-spiking neurons with sound-evoked PSPs. These findings highlight a lack of adaptation for the membrane voltage in those non-adapting neurons that showed low SSA levels in their spiking output.

3.3. Morphological characterization of postsynaptic potentials

We next analyzed the morphological properties of the PSPs evoked in response to standard tones versus deviant tones to study whether those PSPs differed in some features even if the absolute area count was comparable to both conditions. Then, we compared all deviant tones with the last-standard stimuli just before deviant events and next-standard stimuli (i.e., the subsequent tone to deviant events). The adapting neurons with the highest SSA levels had significant differences, such as amplitude, half-width, max rise/decay slope when comparing PSPs evoked by deviant stimuli versus standard stimuli (all standard events together and standard stimuli in specific positions before or after a deviant event, Table 4, Fig. 5). One example is neuron 3 that showed a moderate adapting in the PSPs and very high CSI levels even close to the index maximum for some recording conditions. Interestingly, its analyzed parameters were higher for the PSPs evoked by standard tones (Fig. 5). By contrast, the non-adapting group only showed few differences between deviant and standard events for the same properties and the non-spiking neurons with sound-evoked PSPs presented a small number of differences in some of the parameters.

3.4. Membrane passive properties of neurons of the inferior colliculus

To correlate adaptation properties with passive neuronal properties, we compared these passive membrane properties across groups of cells. Although we did not find significant differences across neuronal groups, there was a tendency for higher capacitance values and smaller membrane resistance in the group of adapting neurons. By contrast, the smallest capacitance values and highest membrane resistances were found in the non-adapting neurons (Table 5).

3.5. Intrinsic properties of neurons of the inferior colliculus

To analyze the intrinsic properties of the IC neurons, we studied the presence of depolarizing sags after the application of hyperpolarizing current pulses. We also analyzed the firing pattern, the interspike interval, the AP threshold and the rebound potential in response to current injection pulses. Two neurons displayed a depolarizing sag; neuron 2 showed a 5 mV sag with a 35 ms tau while neuron 8 showed an 11 mV sag with a 23 ms tau (Fig. 6). These two neurons corresponded to different groups, namely, the adapting and non-spiking neurons with sound-evoked PSPs. Therefore, it was not possible to relate the presence of the sag to any particular neuronal class. Interestingly, it should be mentioned that all the remaining neurons that lacked sags ($n = 8$) had an AP response threshold at a current injection of 100 pA, while the two neurons with sag had a higher AP threshold at 200 pA.

Next, we analyzed the AP firing patterns to investigate whether physiological parameters beyond basic biophysics could serve to characterize the three classes of neurons. Therefore, we calculated the interspike interval and the instantaneous frequency or firing rate at the AP threshold. Only the non-adapted neurons lacked rebound APs. In accord with the firing pattern and interspike interval, neurons were classified as sustained, accommodating, accelerating and burst onset cells (Sivaramakrishnan and Oliver, 2001; Tan et al., 2007). All classes of neurons showed an exponential decrease in their instantaneous frequencies with different behaviors depending on the neuronal type. Sustained neurons showed a gradual/constant decrease in the instantaneous frequency according to its interspike intervals, while the accommodating, accelerating, and burst onset did so in an irregular/non-constant manner (Fig. 6B). The groups of adapting neurons and non-spiking neurons with sound-evoked PSPs showed variability in the types of firing patterns, while the group of non-adapting neurons showed a sustained firing pattern (Fig. 6 & Table 6). Thus, one important difference between adapting and non-adapting neurons is their firing patterns.

4. Discussion

In this study, we have recorded 10 neurons in whole-cell mode in the mouse IC while we applied current injection and sound stimulation under the oddball paradigm. These recordings allowed us to report their passive properties (membrane capacitance, membrane resistance and resting membrane potential), intrinsic properties (firing pattern, AP-threshold, depolarizing sag of hyperpolarizing pulse and rebound AP) and postsynaptic potentials in response to sound stimulation.

The firing pattern of neurons is dependent on the interaction of several voltage-dependent ion conductances (Rutecki, 1992). Within our recording sample, we found that the firing pattern is a key feature to distinguish between adapted and non-adapted neurons. All non-adapted neurons showed a sustained-regular firing, probably due to a high degree of sodium persistent current (Boeri et al., 2018; Chatelier et al., 2010). This type of firing pattern is abundant in CNIC neurons both, *in vitro* (Peruzzi et al., 2000; Sivaramakrishnan and Oliver, 2001) and *in vivo* studies (Tan et al., 2007). CNIC neurons are predominantly non-adapted neurons with the lowest, if any, SSA levels (Malmierca et al., 2009a). By contrast, adapting neurons showed variable firing patterns, including sustained, accommodating and burst onset cells. These types of responses have been shown to be more typical of the cortices of the IC (Geis et al., 2011). These findings conform with our previous works of neurons with higher SSA levels found mainly in the cortices of the IC (Ayala and Malmierca, 2013; Duque et al., 2012; Duque and Malmierca, 2015). Interestingly, we also observed differences between the neuronal receptive fields in their FRAs measurements. FRAs of non-adapting neurons showed typical V-shapes, which is exemplary of the CNIC (Ayala and Malmierca, 2013; Duque et al., 2012; Duque and Malmierca, 2015). By contrast, adapting neurons showed non-V-shaped FRAs without a clear characteristic frequency, which typically belong to the cortices of the IC (Ayala and Malmierca, 2013; Duque et al., 2012; Duque and

Please cite this article as: Valdés-Baizabal, C et al., *In vivo* whole-cell recordings of stimulus-specific adaptation in the inferior colliculus, Hearing Research, https://doi.org/10.1016/j.heares.2020.107978

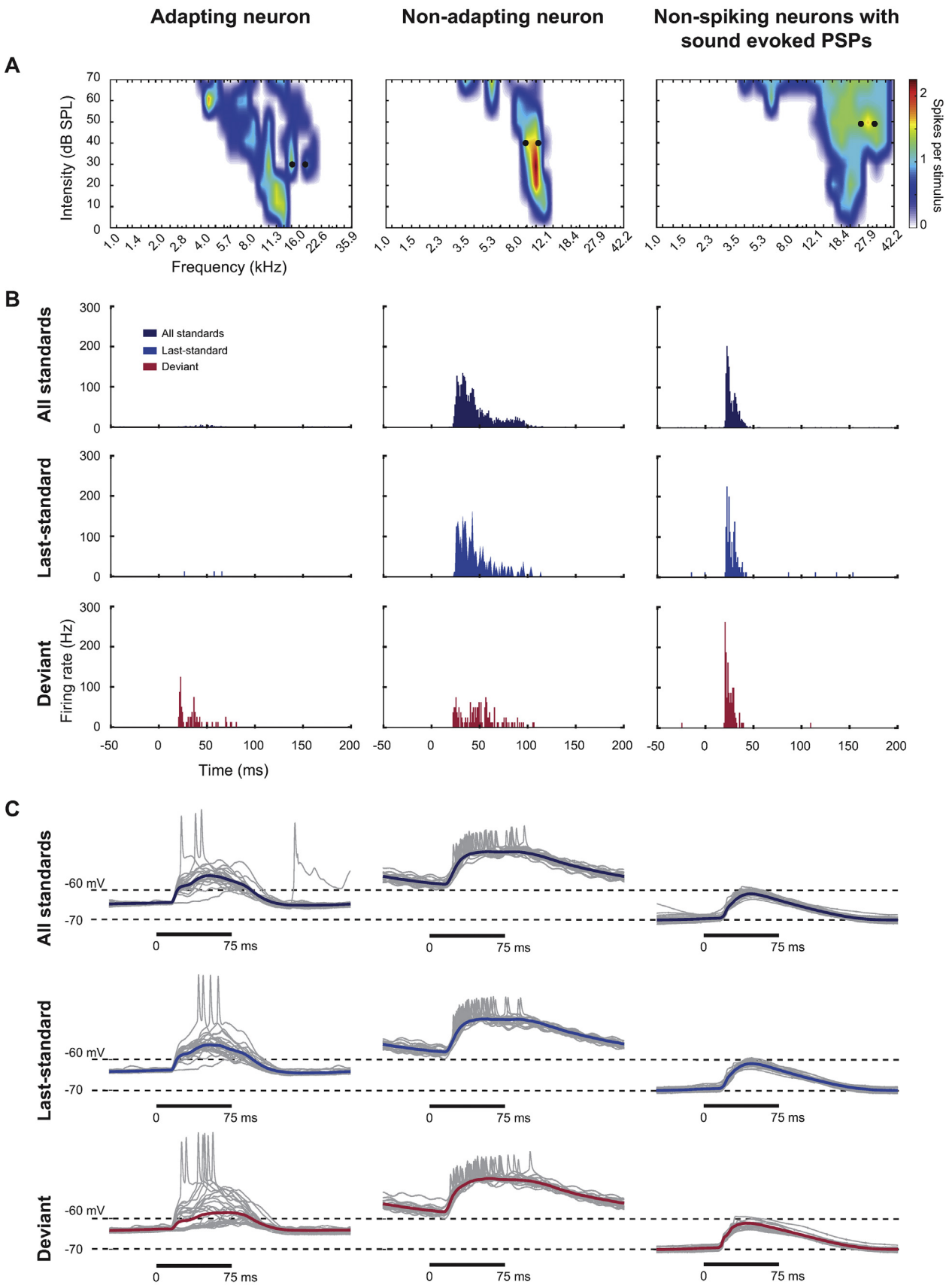

Fig. 3. Examples of an adapting neuron (neuron 3), a non-adapting neuron (neuron 5) and a non-spiking neuron with sound-evoked PSPs (neuron 8). A) Frequency response area for pure tones of a combination of frequencies and intensities. The black dots denote the selected frequencies presented as oddball paradigms. Pure tones lasted 75 ms with an onset-to-onset interval of 250 ms. B) Peristimulus-time histograms of the combined response to the two frequencies presented as each condition: all standard tones (n = 720

Please cite this article as: Valdés-Baizabal, C et al., *In vivo* whole-cell recordings of stimulus-specific adaptation in the inferior colliculus, Hearing Research, https://doi.org/10.1016/j.heares.2020.107978

Table 2
Onset latencies of evoked excitatory areas (EPSPs) and inhibitory areas (IPSPs) for all the recorded stimulus conditions.the

	Neuron #	Onset-to-onset interval (ms)	Tone duration (ms)	Frequencies (KHz)	Intensity (dB SPL)	Deviant	Last-standard	Mean	SEM	Deviant	Last-standard	Mean	SEM
Adapting neurons	1	300	30	11.6 & 14.2	32.5	48.02	45.89	34.15	5.34	40.08	46.58	62.88	7.77
		300	30	10.6 & 15.3	32.5	28.36	30.33			50.49	58.50		
		300	30	16.2 & 19.8	39.5	42.88	36.08			67.71	79.98		
		300	30	14.4 & 20.8	39.5	38.16	88.24			47.32	25.95		
	2	250	75	8.3 & 10.1	43.2	18.30	12.05			78.49	83.11		
	3	250	75	16.2 & 19.8	30.2	14.82	8.48			108.69	124.10		
	4	250	75	13.0 & 16.0	47.2	30.25	36.20			36.96	32.34		
Non-adapting neurons	5	250	75	9.0 & 11.0	39.5	20.12	21.55	29.36	5.28	0.54	0.59	13.96	6.18
		250	75	9.5 & 10.5	39.5	20.30	21.32			0.43	0.22		
		300	30	9.6 & 11.7	25.5	12.90	14.09			1.30	1.13		
		300	30	10.0 & 11.2	25.5	16.68	18.29			2.07	2.45		
		300	30	9.5 & 10.5	39.5	15.40	15.89			1.37	2.30		
	6	300	30	12.7 & 15.5	49.5	59.40	65.24			31.14	24.92		
	7	250	75	18 & 22	20.4	47.22	62.72			61.83	65.16		
Non-spiking neurons with sound-evoked PSPs	8	250	75	25 & 31	48.5	2.53	2.71	19.57	5.77	–	0.1	50.87	12.20
		300	30	21.0 & 26.0	21.5	25.48	7.96			75.19	103.98		
	9	250	75	2.9 & 3.5	57.2	36.78	47.78			43.67	42.48		
	10	250	75	23.3 & 28.4	20.2	19.12	14.18			51.38	39.26		

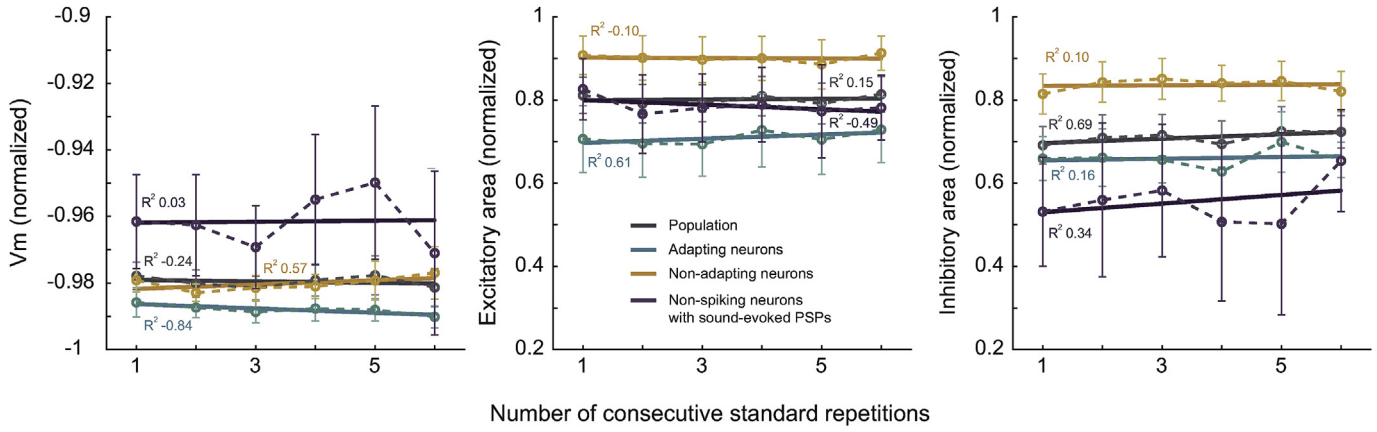

Fig. 4. Correlation between the number of consecutive standard tone presentations and the evoked mean membrane potential, excitatory and inhibitory areas. Data shown as normalized means ± SEM. Linear trends denote the group and population tendency along with adjusted R^2 values, which indicates the goodness of the fit.

Malmierca, 2015).

One possibility for adaptation would be that PSP amplitudes are stable, but the probability of PSPs changes with adaptation, such that adaptation occurs primarily due to decreases in PSP probability. However, the present data demonstrate similarity in the amplitude of sound-evoked PSPs received for each stimulus condition by each neuron, regardless of the degree of spiking adaptation. Because both frequencies selected for the oddball paradigms fell within their receptive field, neurons consistently demonstrated PSPs to both tones. Another possibility, similar to studies in the auditory cortex (Abolafia et al., 2011; Wehr and Zador, 2005), would be that PSP amplitudes and conductances change with adaptation. The analyses of EPSPs and IPSPs separately in this set of neurons do not support this idea and suggest that differences in SSA of synaptic inhibition and excitation are not predictive of spiking SSA levels. Yet another possibility would be changes in the relative timing of inhibition. We observed that inhibition for last-standard stimuli but not for deviant tones was faster for non-adapting neurons than adapting neurons but did not observe changes in IPSP timing related to adaptation. At the 3–4 Hz rate in the present study, although there may be some synaptic depression, it is likely to be weak, on the order of 10–20% (Bartlett and Smith, 2002; Malmierca et al., 2009a; Pérez-González and Malmierca, 2014). However, studies in the IC (Kitagawa and Sakaba, 2019; Malmierca et al., 2009a; Wu et al., 2004) and auditory thalamus (Antunes et al., 2010; Bartlett and Smith, 2002; Venkataraman and Bartlett, 2013) have shown significant synaptic depression that could lead to more prominent SSA and spiking adaptation for faster rates (≥10 Hz).

Previously, it was shown that neurons of the cochlear nucleus and the superior olivary complex lack SSA (Ayala et al., 2013; Duque et al., 2018), while the cortical regions of the IC show strong and robust SSA (Ayala et al., 2013; Lumani and Zhang, 2010; Malmierca

stimulus repetitions), last-standard tones before deviant events (n = 80) and deviant tones (n = 80). Pure tones lasted 75 ms. Bin size: 1 ms. A-B) Frequency response areas and peristimulus-time histograms were computed with the spiking activity for adapting and non-adapting neurons. Responses of the non-spiking neurons with sound-evoked PSPs were computed with the total count of individual PSPs instead of APs since these cells did not fire to the sound stimulation with pure tones. C) Examples of randomly selected traces (gray; n = 25 stimulus repetitions) and average membrane potential responses of all stimulus repetitions after removing action potentials (colored) in the same neurons. This shows how the frequency tones were selected and the time-locked activity to deviant and standard tones.

Please cite this article as: Valdés-Baizabal, C et al., *In vivo* whole-cell recordings of stimulus-specific adaptation in the inferior colliculus, Hearing Research, https://doi.org/10.1016/j.heares.2020.107978

Table 3
Comparison between number of standard repetitions and evoked responses in the mean membrane potential (Vm), excitatory areas (EPSPs) and inhibitory areas (IPSPs).

	Neuron #	Mean Vm	EPSP	IPSP
Adapting neurons	1	1^{st}, 2^{nd} & 3^{rd} standards different than 4^{th} to 9^{th} 4^{th} standard different than 5^{th} to 9^{th} 5^{th}standard different than 6^{th} to 8^{th} $_{6th}$ standard different than 7th & 8_{th} 7^{th} standard different than 8^{th} & 9^{th} 8^{th} standard different than 9^{th} ($p < 0.001$)	1^{st}, 2^{nd} & 3^{rd} standards different than 5^{th} to 7^{th} 4^{th} standard different than 6^{th} & 7^{th} 6^{th} standard different than 8^{th}($p < 0.001$)	1^{st} standard different than the 7^{th} ($p = 0.001$)
	2	1^{st}standard different than the 6^{th} ($p < 0.001$)	$p = 0.779$	1^{st} standard different than the 7^{th} ($p < 0.001$)
	3	1^{st} standard different than the rest 6^{th} standard different than 1st to 4^{th} 7^{th} standard different than 1^{st} to 5^{th} ($p < 0.001$)	7^{th} & 8^{th} standards different than 1st to 4th ($p < 0.001$) 4^{th} standard different than 6th $p = 0.002$	9^{th} standard different than the 5th to 7th ($p < 0.001$)
	4	$p = 0.484$	$p = 0.788$	$p = 0.783$
Non-adapting neurons	5	$p = 0.824$	$p = 0.161$	$p = 0.072$
	6	$p = 0.662$	$p = 0.984$	$p = 0.688$
	7	7^{th} standard different than 2^{nd} & 3^{rd} 8^{th} standard different than the rest ($p < 0.001$)	8^{th} standard different than the rest ($p < 0.001$)	8^{th} standard different than the rest ($p < 0.001$)
Non-spiking neurons with sound-evoked PSPs	8	6^{th} and 7^{th} standards different than 1st to 3rd ($p < 0.001$)	$p = 0.039$; No significant post hoc comparison.	$p = 0.066$
	9	$p = 0.038$; Non-significant post hoc comparisons	$p = 0.848$	$p = 0.997$
	10	1^{st} standard different than the 2nd ($p = 0.003$) & 3^{rd} ($p = 0.021$)	$p = 0.607$	$p = 0.676$

One-Way ANOVA and post hoc pairwise multiple comparisons procedures with the Holm-Sidak method.

Table 4
Summary of the analyzed parameters of post-synaptic potentials compared between deviant and standard stimuli.

		Adapting neurons		Non-adapting neurons	Non-spiking neurons with sound-evoked PSPs	
Parameter	Comparison	Neuron #				
		2	3	5	8	10
Amplitude	STD vs. DEV	$p < 0.001$	$p < 0.001$	n.s.	$p < 0.001$	n.s.
	last-STD vs. DEV	$p < 0.001$	$p < 0.001$	n.s.	$p < 0.001$	n.s.
	next-STD vs. DEV	$p < 0.001$	$p < 0.001$	n.s.	$p < 0.001$	n.s.
	last-STD vs. next-STD	n.s.	n.s.	n.s.	$p < 0.001$	n.s.
Half-width	STD vs. DEV	n.s.	$p < 0.001$	$p < 0.05$	n.s.	$p < 0.05$
	last-STD vs. DEV	n.s.	$p < 0.001$	n.s.	n.s.	n.s.
	next-STD vs. DEV	n.s.	$p < 0.001$	$p < 0.001$	$p < 0.001$	$p < 0.05$
	last-STD vs. next-STD	n.s.	n.s.	n.s.	n.s.	n.s.
Max Rise Slope	STD vs. DEV	n.s.	$p < 0.001$	$p < 0.05$	$p < 0.001$	$p < 0.05$
	last-STD vs. DEV	$p < 0.001$	$p < 0.001$	n.s.	$p < 0.001$	n.s.
	next-STD vs. DEV	$p = 0.004$	$p < 0.001$	n.s.	$p < 0.001$	n.s.
	last-STD vs. next-STD	n.s.	n.s.	n.s.	n.s.	n.s.
Max Decay Slope	STD vs. DEV	n.s.	$p < 0.001$	n.s.	n.s.	$p < 0.05$
	last-STD vs. DEV	n.s.	$p < 0.001$	n.s.	n.s.	n.s.
	next-STD vs. DEV	n.s.	$p < 0.001$	$p < 0.05$	n.s.	n.s.
	last-STD vs. next-STD	n.s.	n.s.	n.s.	n.s.	n.s.
Rise Slope 10%–90%	STD vs. DEV	$p < 0.005$	$p < 0.005$	n.s.	$p < 0.001$	n.s.
	last-STD vs. DEV	$p < 0.05$	$p < 0.05$	n.s.	$p < 0.001$	n.s.
	next-STD vs. DEV	$p < 0.05$	$p < 0.05$	n.s.	$p < 0.001$	n.s.
	last-STD vs. next-STD	n.s.	n.s.	n.s.	n.s.	n.s.
Rise Time 10%–90%	STD vs. DEV	n.s.	$p < 0.005$	$p < 0.05$	$p < 0.05$	n.s.
	last-STD vs. DEV	n.s.	$p < 0.05$	n.s.	n.s.	n.s.
	next-STD vs. DEV	n.s.	$p < 0.05$	n.s.	n.s.	n.s.
	last-STD vs. next-STD	n.s.	n.s.	n.s.	n.s.	n.s.
Decay Slope 90%–10%	STD vs. DEV	n.s.	$p < 0.005$	n.s.	$p < 0.001$	n.s.
	last-STD vs. DEV	n.s.	$p < 0.05$	n.s.	$p < 0.001$	n.s.
	next-STD vs. DEV	n.s.	$p < 0.05$	n.s.	$p < 0.001$	n.s.
	last-STD vs. next-STD	n.s.	n.s.	n.s.	n.s.	n.s.
Decay Time 90%–10%	STD vs. DEV	n.s.	n.s.	n.s.	$p < 0.05$	n.s.
	last-STD vs. DEV	n.s.	n.s.	n.s.	$p < 0.05$	n.s.
	next-STD vs. DEV	n.s.	n.s.	n.s.	$p < 0.05$	n.s.
	last-STD vs. Next-STD	n.s.	n.s.	n.s.	n.s.	n.s.

Comparisons were performed between standard events (all standard tones [STD], last-standard tones before deviant events [last-STD] and next-standard tones after a deviant event [next-STD]) and deviant tones (DEV). n.s. means a non-statistically significant difference. One-Way Repeated-Measures ANOVA. Neurons that did not show significant changes in any comparison are not included in the table to facilitate visualization.

Please cite this article as: Valdés-Baizabal, C et al., *In vivo* whole-cell recordings of stimulus-specific adaptation in the inferior colliculus, Hearing Research, https://doi.org/10.1016/j.heares.2020.107978

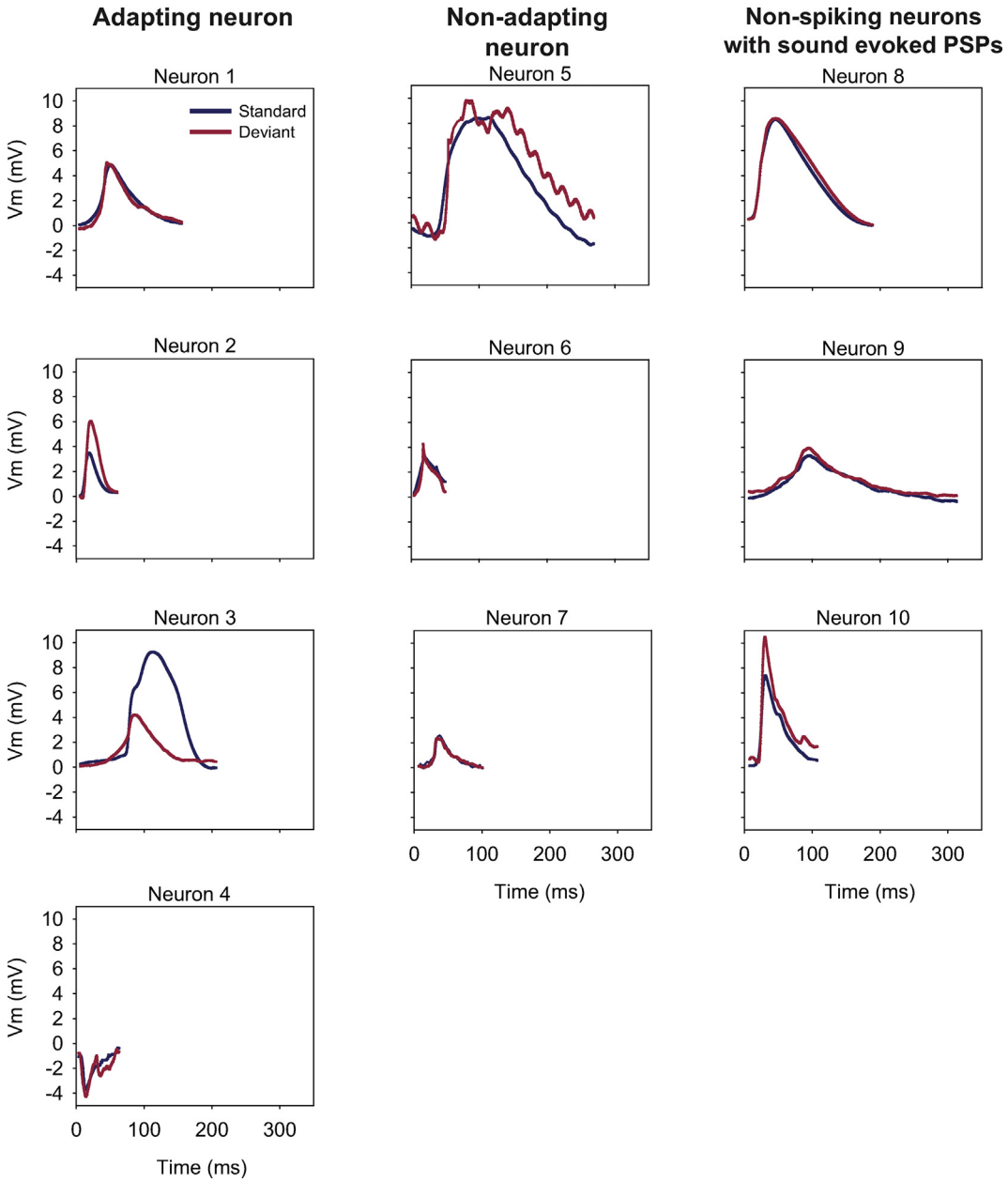

Fig. 5. Mean post-synaptic potentials from each adapting, non-adapting and non-spiking neurons with sound-evoked PSPs. For morphological analyses, postsynaptic potentials were aligned to its maximum peak for excitatory postsynaptic potentials or minimum peak for inhibitory postsynaptic potentials.

Table 5
Membrane passive properties of IC neurons.

	Neuron #	Capacitance (pF)		Membrane resistance (MΩ)		Resting membrane potential (mV)	
		Individual	Mean	Individual	Mean	Individual	Mean
Adapting neurons	1	13	12.75 ± 2.95	660	434 ± 91.89	−45	−56 ± 6.67
	2	21		212		−69	
	3	9		410		−66	
	4	8		454		−44	
Non-adapting neurons	5	3	9.33 ± 4.48	707	769 ± 40.45	−55	−52.67 ± 2.85
	6	7		755		−47	
	7	18		845		−56	
Non-spiking neurons with sound-evoked PSPs	8	2	7.67 ± 4.26	486	463.67 ± 124.34	−66	−65.33 ± 0.33
	9	16		667		−65	
	10	5		238		−65	
p-values		0.433		0.222		0.481	

Average ± SEM; n = 4 adapting neurons, 3 non-adapting neurons & 3 non-spiking neurons with sound-evoked PSPs; One-Way Repeated-Measures ANOVA.

Please cite this article as: Valdés-Baizabal, C et al., *In vivo* whole-cell recordings of stimulus-specific adaptation in the inferior colliculus, Hearing Research, https://doi.org/10.1016/j.heares.2020.107978

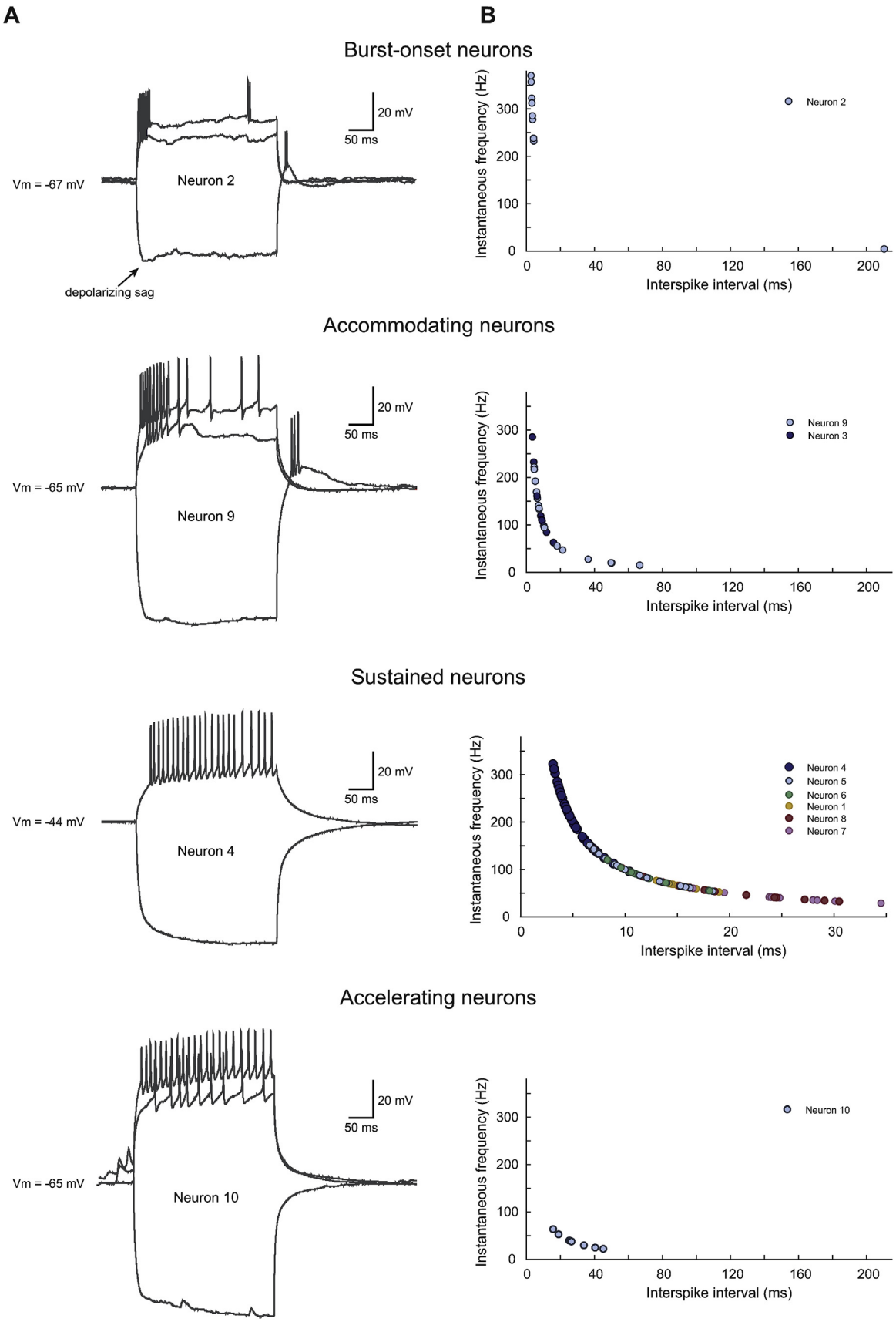

Fig. 6. Example of each type of firing pattern found in the IC neurons. A) Membrane voltage traces under injection of square current pulse series. The most hyperpolarizing current pulse, the depolarizing pulse at the AP threshold and the pulse 100 pA above it are shown. Neurons 2 and 4 are adapting neurons and neurons 8 and 9 are non-spiking neurons with sound-evoked PSPs. B) Interspike interval versus instantaneous frequency of all neurons calculated 100 pA above AP threshold.

Please cite this article as: Valdés-Baizabal, C et al., *In vivo* whole-cell recordings of stimulus-specific adaptation in the inferior colliculus, Hearing Research, https://doi.org/10.1016/j.heares.2020.107978

Table 6
Classification of types of firing patterns in number of IC neurons within each group .

	Adapting neurons	Non-adapting neurons	Non-spiking neurons with sound-evoked PSPs
Sustained	2	3	1
Accommodating	1		1
Accelerating			1
Burst onset	1		

Adapting neurons, non-adapting neurons and non-spiking neurons with sound-evoked PSPs were classified according to their AP discharge to depolarizing and hyperpolarizing current injections.

et al., 2009a; Pérez-González et al., 2005; Zhao et al., 2011) with extracellular recordings of single units in anesthetized and awake rodents (Duque and Malmierca, 2015) and with brainstem auditory evoked potentials (Duque et al., 2018). These results suggest that SSA emerges at the level of the IC and is prevalent in IC cortex. Thus, the question arises whether spiking adaptation results from PSP adaptation in the IC. Neurons in IC cortex receive ascending auditory inputs, inputs from other IC neurons and auditory cortex (Cant and Oliver, 2018; Ito and Malmierca, 2018; Loftus et al., 2008; Malmierca, 2015; Malmierca et al., 2009b, 2005, 1995; Malmierca and Ryugo, 2012). Our set of IC neurons suggests that synaptic adaptation was variable, with weak or no SSA in some neurons, clear synaptic SSA in a couple of neurons, and even reduced deviant EPSP amplitude coupled with spiking SSA (Fig. 5). This finding extended to both adapting and non-adapting neurons and suggests that synaptic adaptation could not be used to predict the presence of spiking SSA. This finding differs from auditory cortical evidence, where SSA was observed at subthreshold level, both *in vivo* (Chen et al., 2015; Hershenhoren et al., 2014) and *in vitro* (Wang et al., 2014) due to synaptic depression of thalamocortical projections (Chung et al., 2002; Katz et al., 2006). Indeed, the lack of synaptic SSA in the IC further supports previous work where the auditory cortex was deactivated, which did not eliminate subcortical SSA (Anderson and Malmierca, 2013; Antunes and Malmierca, 2011). Thus, the present study further supports the notion that the non-lemniscal IC is the first site at the auditory pathway where SSA emerges.

We observed a small trend towards hyperpolarized membrane potentials in adapting neurons and increased synaptic inhibition with an increasing number of standard repetitions at the population level. This finding denotes a moderate level of adaptation only observed when one stimulus is consecutively repeated. Since we detected these trends of a small increase at the population level, it does not seem to explain the SSA levels observed at the AP activity. This result suggests a more simple type of adaptation related to potassium conductances. Potassium conductances have been associated with adaptation on a scale of seconds to minutes. It is known that potassium conductances contribute to sensory adaptation in sensorimotor, barrel and visual cortices (Díaz-Quesada and Maravall, 2008; Sanchez-Vives et al., 2000a, 2000b; Schwindt et al., 1988; Wang et al., 2003). The activation of potassium currents hyperpolarizes the membrane potential, decreasing the neuronal responsiveness to subsequent synaptic inputs with time courses ranging from tens of milliseconds to tens of seconds. Such slow time courses are supported by the dynamics of the relevant intracellular ions, in particular, Na^+, in the vicinity of K^+ channels and their binding/unbinding to them (Abolafia et al., 2011). The depolarization and high-frequency firing during sensory responses induce not only the activation of voltage-dependent potassium currents but also an intracellular increase of ions like Ca^{2+} and Na^+ that activate ion-dependent K^+ channels (for reviews see Bhattacharjee and Kaczmarek, 2005; Sah and Faber, 2002). This cascade of events occurs equally for all stimulus conditions and can explain similarities among responses.

Adapted/non-spiking and non-adapted neurons differ by the appearance of a rebound depolarization after cessation of hyperpolarization, leading to rebound firing. Specifically, only the non-adapted neurons lacked rebound depolarization and rebound APs. *In vivo*, rebound depolarizations can be evoked by inhibitory synaptic stimuli. The ion channels usually believed to underlie rebound depolarizations are the low voltage activated T-type (Ca_{V3}) calcium channels and hyperpolarization-activated HCN channels (Jahnsen and Llinás, 1984; Molineux et al., 2008). For example, in the medial geniculate body of the rat, it is carried by T-type Ca^{2+} channels, and regulated by HCN channels and likely GIRK channels by changing the resting potential (Wang et al., 2016). These findings could indicate differences in the intrinsic properties of adapted and non-adapted neurons but some experimental strategies such as pharmacological and voltage-clamp mode recordings are needed to disentangle specific ionic channels' contributions. Two cells demonstrated a slight depolarizing sag followed by a rebound action potential suggesting the presence of hyperpolarization-activated current (I_h; Nagtegaal and Borst, 2010). However, given the membrane potential, it could be due to inward rectifier K^+ channels. We could not conclude the role of the depolarizing sag into SSA. Only one neuron classified as adapting and the other lacked sound-evoked spikes and therefore, its SSA level could not be determined.

Although our work represents a first and important step in the study of intracellular responses of SSA neurons *in vivo* in the IC, our conclusions should be considered as example case reports and be strengthened by further studies, increasing the number of intracellularly recorded neurons. It is widely accepted that blind whole-cell patch-clamp is a laborious technique with a low yield, especially *in vivo* using adult animals; success rates are ~25% of the attempts even with automated methods (Kodandaramaiah et al., 2012; Margrie et al., 2002). In our study design, we required a considerable stable time of recording of about 10 min combining the current stimulation and sound stimulation with FRAs, and the selection of two frequencies for at least two oddball sequences. Another limiting factor is that the group of non-spiking neurons with sound-evoked PSPs is difficult to integrate within this study due to the lack of tone-evoked spikes and, therefore, it precludes comparison with classical extracellular spike counts used to compute CSI levels. As a result, these neurons have not been studied classically with extracellular recordings and their auditory adaptation levels are unknown. Here, we can only establish the adaptation properties at their PSPs. In line with previous research, cells without tone-evoked APs have been found in the mouse CNIC *in vivo* (Tan et al., 2007), in the mouse dorsal cortex where the ratio of these neurons was higher with around half of the recorded cells (Geis et al., 2011), in the rat dorsal cortex (Lumani and Zhang, 2010) and even in the primary auditory cortex (Hershenhoren et al., 2014). Hence, this preliminary piece of work will need to be expanded in future studies with a higher population number and more in-depth types of manipulations such as injections of depolarizing currents forcing AP firing in non-spiking neurons to pure tones or more complex forms of auditory stimuli.

Please cite this article as: Valdés-Baizabal, C et al., *In vivo* whole-cell recordings of stimulus-specific adaptation in the inferior colliculus, Hearing Research, https://doi.org/10.1016/j.heares.2020.107978

5. Conclusion

In this study, we have made the first attempt to correlate some neuronal electrophysiological properties of adapting, non-adapting neurons and non-spiking neurons with sound-evoked PSPs. We demonstrated the similarity of excitatory or inhibitory synaptic inputs that each neuron receives regardless of their SSA properties at the spiking activity. Although a couple of the adapting neurons had synaptics that differed between deviant and standard stimuli, that was not necessary to produce spiking SSA. Thus, synaptic SSA was variable and could not be used to predict the presence of spiking SSA. Our data suggest that intrinsic properties differ between adapting and non-adapting neurons since they displayed different firing patterns (Fig. 6 and Table 6). Our results suggest that intrinsic properties (probably potassium conductances) may contribute to classifying neurons as adapting or non-adapting ones. Therefore, in future studies, it would be worth analyzing in more detail the properties and distributions of these potassium channels. Finally, we should emphasize that the conclusions drawn from this study are modest as our sample is very small, but they show the potential for future studies of this type to understand how SSA is generated at the cellular level.

Declaration of competing interest

The authors declare no competing interests.

CRediT authorship contribution statement

Catalina Valdés-Baizabal: Conceptualization, Methodology, Investigation, Formal analysis, Visualization, Writing - original draft, Writing - review & editing. **Lorena Casado-Román:** Conceptualization, Methodology, Software, Formal analysis, Visualization, Writing - original draft, Writing - review & editing. **Edward L. Bartlett:** Conceptualization, Writing - review & editing. **Manuel S. Malmierca:** Conceptualization, Writing - review & editing, Supervision, Project administration, Funding acquisition.

Acknowledgments

We thank Drs. Doug Oliver, H. Rüdiger A.P. Geis, J. Gerard G. Borst and Aaron B. Wong for the experimental assistance and/or advice. We also thank Mr. Ignacio Plaza for helping with the histological staining. Funding: this project received funding from the Spanish MINECO [grant number SAF2016-75803-P] and the European Union's Horizon 2020 research and innovation programme under the Marie Skłodowska-Curie LISTEN [grant number 722098] to MSM. CVB held a fellowship from the Mexican National Council of Science and Technology [grant number 216652].

References

Abolafia, J.M., Vergara, R., Arnold, M.M., Reig, R., Sanchez-Vives, M.V., 2011. Cortical auditory adaptation in the awake rat and the role of potassium currents. Cerebr. Cortex 21, 977–990. https://doi.org/10.1093/cercor/bhq163.

Almanza, A., Luis, E., Mercado, F., Vega, R., Soto, E., 2012. Molecular identity, ontogeny, and cAMP modulation of the hyperpolarization-activated current in vestibular ganglion neurons. J. Neurophysiol. 108, 2264–2275. https://doi.org/10.1152/jn.00337.2012.

Anderson, L.A., Malmierca, M.S., 2013. The effect of auditory cortex deactivation on stimulus-specific adaptation in the inferior colliculus of the rat. Eur. J. Neurosci. 37, 52–62. https://doi.org/10.1111/ejn.12018.

Antunes, F.M., Malmierca, M.S., 2011. Effect of auditory cortex deactivation on stimulus-specific adaptation in the medial geniculate body. J. Neurosci. 31, 17306–17316. https://doi.org/10.1523/JNEUROSCI.1915-11.2011.

Antunes, F.M., Nelken, I., Covey, E., Malmierca, M.S., 2010. Stimulus-specific adaptation in the auditory thalamus of the anesthetized rat. PloS One 5, e14071. https://doi.org/10.1371/journal.pone.0014071.

Ayala, Y.A., Malmierca, M.S., 2018. The effect of inhibition on stimulus-specific adaptation in the inferior colliculus. Brain Struct. Funct. 223, 1391–1407. https://doi.org/10.1007/s00429-017-1546-4.

Ayala, Y.A., Malmierca, M.S., 2015. Cholinergic modulation of stimulus-specific adaptation in the inferior colliculus. J. Neurosci. 35, 12261–12272. https://doi.org/10.1523/JNEUROSCI.0909-15.2015.

Ayala, Y.A., Malmierca, M.S., 2013. Stimulus-specific adaptation and deviance detection in the inferior colliculus. Front. Neural Circ. 6, 1–16. https://doi.org/10.3389/fncir.2012.00089.

Ayala, Y.A., Pérez-González, D., Duque, D., Nelken, I., Malmierca, M.S., 2013. Frequency discrimination and stimulus deviance in the inferior colliculus and cochlear nucleus. Front. Neural Circ. 6, 1–19. https://doi.org/10.3389/fncir.2012.00119.

Ayala, Y.A., Pérez-González, D., Malmierca, M.S., 2016. Stimulus-specific adaptation in the inferior colliculus: the role of excitatory, inhibitory and modulatory inputs. Biol. Psychol. 116, 10–22. https://doi.org/10.1016/j.biopsycho.2015.06.016.

Ayala, Y.A., Udeh, A., Dutta, K., Bishop, D., Malmierca, M.S., Oliver, D.L., 2015. Differences in the strength of cortical and brainstem inputs to SSA and non-SSA neurons in the inferior colliculus. Sci. Rep. 5, 1–17. https://doi.org/10.1038/srep10383.

Bartlett, E.L., Smith, P.H., 2002. Effects of paired-pulse and repetitive stimulation on neurons in the rat medial geniculate body. Neuroscience 113, 957–974. https://doi.org/10.1016/s0306-4522(02)00240-3.

Bhattacharjee, A., Kaczmarek, L.K., 2005. For K+ channels, Na+ is the new Ca2+. Trends Neurosci. https://doi.org/10.1016/j.tins.2005.06.003.

Boeri, J., Le Corronc, H., Lejeune, F.X., Le Bras, B., Mouffle, C., Angelim, M.K.S.C., Mangin, J.M., Branchereau, P., Legendre, P., Czarnecki, A., 2018. Persistent sodium current drives excitability of immature renshaw cells in early embryonic spinal networks. J. Neurosci. 38, 7667–7682. https://doi.org/10.1523/JNEUROSCI.3203-17.2018.

Brandt, H.M., Apkarian, A.V., 1992. Biotin-dextran: a sensitive anterograde tracer for neuroanatomic studies in rat and monkey. J. Neurosci. Methods 45, 35–40. https://doi.org/10.1016/0165-0270(92)90041-b.

Cant, N.B., Oliver, D.L., 2018. Overview of auditory projection pathways and intrinsic microcircuits. In: The Mammalian Auditory Pathways, vol. 65. Springer, Cham, pp. 7–39. https://doi.org/10.1007/978-3-319-71798-2_6. Springer Handbook of Auditory Research.

Chatelier, A., Zhao, J., Bois, P., Chahine, M., 2010. Biophysical characterisation of the persistent sodium current of the Nav1.6 neuronal sodium channel: a single-channel analysis. Pflugers Arch. Eur. J. Physiol. 460, 77–86. https://doi.org/10.1007/s00424-010-0801-9.

Chen, I.-W., Helmchen, F., Lutcke, H., 2015. Specific early and late oddball-evoked responses in excitatory and inhibitory neurons of mouse auditory cortex. J. Neurosci. 35, 12560–12573. https://doi.org/10.1523/JNEUROSCI.2240-15.2015.

Chung, S., Li, X., Nelson, S.B., 2002. Short-term depression at thalamocortical synapses contributes to rapid adaptation of cortical sensory responses in vivo. Neuron 34, 437–446. https://doi.org/10.1016/S0896-6273(02)00659-1.

Díaz-Quesada, M., Maravall, M., 2008. Intrinsic mechanisms for adaptive gain rescaling in barrel cortex. J. Neurosci. 28, 696–710. https://doi.org/10.1523/JNEUROSCI.4931-07.2008.

Duque, D., Malmierca, M.S., 2015. Stimulus-specific adaptation in the inferior colliculus of the mouse: anesthesia and spontaneous activity effects. Brain Struct. Funct. 220, 3385–3398. https://doi.org/10.1007/s00429-014-0862-1.

Duque, D., Pais, R., Malmierca, M.S., 2018. Stimulus-specific adaptation in the anesthetized mouse revealed by brainstem auditory evoked potentials. Hear. Res. 370, 294–301. https://doi.org/10.1016/j.heares.2018.08.011.

Duque, D., Pérez-González, D., Ayala, Y.A., Palmer, A.R., Malmierca, M.S., 2012. Topographic distribution, frequency, and intensity dependence of stimulus-specific adaptation in the inferior colliculus of the rat. J. Neurosci. 32, 17762–17774. https://doi.org/10.1523/JNEUROSCI.3190-12.2012.

Duque, D., Wang, X., Nieto-Diego, J., Krumbholz, K., Malmierca, M.S., 2016. Neurons in the inferior colliculus of the rat show stimulus-specific adaptation for frequency, but not for intensity. Sci. Rep. 6, 1–15. https://doi.org/10.1038/srep24114.

Flecknell, P., 2009. In: Laboratory Animal Anaesthesia (Ed.), Laboratory Animal Anaesthesia, third ed. Elsevier. https://doi.org/10.1016/B978-0-12-369376-1.X0001-9.

Geis, H.R., Borst, J.G.G., 2013. Large GABAergic neurons form a distinct subclass within the mouse dorsal cortex of the inferior colliculus with respect to intrinsic properties, synaptic inputs, sound responses, and projections. J. Comp. Neurol. 521, 189–202. https://doi.org/10.1002/cne.23170.

Geis, H.R., Borst, J.G.G., 2009. Intracellular responses of neurons in the mouse inferior colliculus to sinusoidal amplitude-modulated tones. J. Neurophysiol. 101, 2002–2016. https://doi.org/10.1152/jn.90966.2008.

Geis, H.R., van der Heijden, M., Borst, J.G.G., 2011. Subcortical input heterogeneity in the mouse inferior colliculus. J. Physiol. 589, 3955–3967. https://doi.org/10.1113/jphysiol.2011.210278.

Hernández, O., Espinosa, N., Pérez-González, D., Malmierca, M.S., 2005. The inferior colliculus of the rat: a quantitative analysis of monaural frequency response areas. Neuroscience 132, 203–217. https://doi.org/10.1016/j.neuroscience.2005.01.001.

Hershenhoren, I., Taaseh, N., Antunes, F.M., Nelken, I., 2014. Intracellular correlates of stimulus-specific adaptation. J. Neurosci. 34, 3303–3319. https://doi.org/10.1523/JNEUROSCI.2166-13.2014.

Ito, T., Malmierca, M.S., 2018. Neurons, connections, and microcircuits of the inferior colliculus. In: The Mammalian Auditory Pathways, vol. 65. Springer, Cham,

pp. 127–167. https://doi.org/10.1007/978-3-319-71798-2_6. Springer Handbook of Auditory Research.

Jahnsen, H., Llinás, R., 1984. Ionic basis for the electro-responsiveness and oscillatory properties of Guinea-pig thalamic neurones in vitro. J. Physiol. 349, 227–247. https://doi.org/10.1113/jphysiol.1984.sp015154.

Katz, Y., Heiss, J.E., Lampl, I., 2006. Cross-whisker adaptation of neurons in the rat barrel cortex. J. Neurosci. 26, 13363–13372. https://doi.org/10.1523/JNEUROSCI.4056-06.2006.

Kitagawa, M., Sakaba, T., 2019. Developmental changes in the excitatory short-term plasticity at input synapses in the rat inferior colliculus. Eur. J. Neurosci. 50, 2830–2846. https://doi.org/10.1111/ejn.14422.

Kodandaramaiah, S.B., Franzesi, G.T., Chow, B.Y., Boyden, E.S., Forest, C.R., 2012. Automated whole-cell patch-clamp electrophysiology of neurons in vivo. Nat. Methods 9, 585–587. https://doi.org/10.1038/nmeth.1993.

Kuwada, S., Batra, R., Yin, T.C., Oliver, D.L., Haberly, L.B., Stanford, T.R., 1997. Intracellular recordings in response to monaural and binaural stimulation of neurons in the inferior colliculus of the cat. J. Neurosci. 17, 7565–7581. https://doi.org/10.1523/JNEUROSCI.17-19-07565.1997.

Loftus, W.C., Malmierca, M.S., Bishop, D.C., Oliver, D.L., 2008. The cytoarchitecture of the inferior colliculus revisited: a common organization of the lateral cortex in rat and cat. Neuroscience 154, 196–205. https://doi.org/10.1016/j.neuroscience.2008.01.019.

Lumani, A., Zhang, H., 2010. Responses of neurons in the rat's dorsal cortex of the inferior colliculus to monaural tone bursts. Brain Res. 1351, 115–129. https://doi.org/10.1016/j.brainres.2010.06.066.

Ma, C.L., Kelly, J.B., Wu, S.H., 2002. AMPA and NMDA receptors mediate synaptic excitation in the rat's inferior colliculus. Hear. Res. 168, 25–34. https://doi.org/10.1016/s0378-5955(02)00370-2.

Malinowski, S.T., Wolf, J., Kuenzel, T., 2019. Intrinsic and synaptic dynamics contribute to adaptation in the core of the avian central nucleus of the inferior colliculus. Front. Neural Circ. 13, 46. https://doi.org/10.3389/fncir.2019.00046.

Malmierca, M.S., 2015. Auditory system. In: Paxinos, G. (Ed.), The Rat Nervous System. Academic Press, Amsterdam, pp. 865–946.

Malmierca, M.S., Blackstad, T.W., Osen, K.K., 2011. Computer-assisted 3-D reconstructions of Golgi-impregnated neurons in the cortical regions of the inferior colliculus of rat. Hear. Res. 274, 13–26. https://doi.org/10.1016/j.heares.2010.06.011.

Malmierca, M.S., Blackstad, T.W., Osen, K.K., Karagülle, T., Molowny, R.L., 1993. The central nucleus of the inferior colliculus in rat: a Golgi and computer reconstruction study of neuronal and laminar structure. J. Comp. Neurol. 333, 1–27. https://doi.org/10.1002/cne.903330102.

Malmierca, M.S., Cristaudo, S., Pérez-González, D., Covey, E., 2009a. Stimulus-specific adaptation in the inferior colliculus of the anesthetized rat. J. Neurosci. 29, 5483–5493. https://doi.org/10.1523/JNEUROSCI.4153-08.2009.

Malmierca, M.S., Hernández, O., Antunes, F.M., Rees, A., 2009b. Divergent and point-to-point connections in the commissural pathway between the inferior colliculi. J. Comp. Neurol. 514, 226–239. https://doi.org/10.1002/cne.21997.

Malmierca, M.S., Niño-Aguillón, B.E., Nieto-Diego, J., Porteros, Á., Pérez-González, D., Escera, C., 2019. Pattern-sensitive neurons reveal encoding of complex auditory regularities in the rat inferior colliculus. Neuroimage 184, 889–900. https://doi.org/10.1016/j.neuroimage.2018.10.012.

Malmierca, M.S., Rees, A., Le Beau, F.E.N., Bjaalie, J.G., 1995. Laminar organization of frequency-defined local axons within and between the inferior colliculi of the Guinea pig. J. Comp. Neurol. 357, 124–144. https://doi.org/10.1002/cne.903570112.

Malmierca, M.S., Ryugo, D.K., 2012. Cortical Descending Projections to Auditory Midbrain and Brainstem. The Auditory Cortex. Springer-Verlag, San Diego.

Malmierca, M.S., Saint Marie, R.L., Merchan, M.A., Oliver, D.L., 2005. Laminar inputs from dorsal cochlear nucleus and ventral cochlear nucleus to the central nucleus of the inferior colliculus: two patterns of convergence. Neuroscience 136, 883–894. https://doi.org/10.1016/j.neuroscience.2005.04.040.

Margrie, T.W., Brecht, M., Sakmann, B., 2002. In vivo, low-resistance, whole-cell recordings from neurons in the anaesthetized and awake mammalian brain. Pflugers Arch. Eur. J. Physiol. 444, 491–498. https://doi.org/10.1007/s00424-002-0831-z.

Molineux, M.L., Mehaffey, W.H., Tadayonnejad, R., Anderson, D., Tennent, A.F., Turner, R.W., 2008. Ionic factors governing rebound burst phenotype in rat deep cerebellar neurons. J. Neurophysiol. 100, 2684–2701. https://doi.org/10.1152/jn.90427.2008.

Movshon, J.A., Lennie, P., 1979. Pattern-selective adaptation in visual cortical neurones. Nature 278, 850–852. https://doi.org/10.1038/278850a0.

Nagtegaal, A.P., Borst, J.G.G., 2010. In vivo dynamic clamp study of Ih in the mouse inferior colliculus. J. Neurophysiol. 104, 940–948. https://doi.org/10.1152/jn.00264.2010.

Neher, E., 1992. Correction for liquid junction potentials in patch clamp experiments. Methods Enzymol. 207, 123–131. https://doi.org/10.1016/0076-6879(92)07008-c.

Pérez-González, D., Hernández, O., Covey, E., Malmierca, M.S., 2012. GABA A-mediated inhibition modulates stimulus-specific adaptation in the inferior colliculus. PloS One 7. https://doi.org/10.1371/journal.pone.0034297.

Pérez-González, D., Malmierca, M.S., 2014. Adaptation in the auditory system: an overview. Front. Integr. Neurosci. https://doi.org/10.3389/fnint.2014.00019.

Pérez-González, D., Malmierca, M.S., Covey, E., 2005. Novelty detector neurons in the mammalian auditory midbrain. Eur. J. Neurosci. 22, 2879–2885. https://doi.org/10.1111/j.1460-9568.2005.04472.x.

Peruzzi, D., Sivaramakrishnan, S., Oliver, D.L., 2000. Identification of cell types in brain slices of the inferior colliculus. Neuroscience 101, 403–416. https://doi.org/10.1016/s0306-4522(00)00382-1.

Rabang, C.F., Parthasarathy, A., Venkataraman, Y., Fisher, Z.L., Gardner, S.M., Bartlett, E.L., 2012. A computational model of inferior colliculus responses to amplitude modulated sounds in young and aged rats. Front. Neural Circ. 6, 77. https://doi.org/10.3389/fncir.2012.00077.

Rutecki, P.A., 1992. Neuronal excitability: voltage-dependent currents and synaptic transmission. J. Clin. Neurophysiol. 9, 195–211.

Sah, P., Faber, E.S.L., 2002. Channels underlying neuronal calcium-activated potassium currents. Prog. Neurobiol. 66, 345–353. https://doi.org/10.1016/s0301-0082(02)00004-7.

Sanchez-Vives, M.V., Nowak, L.G., McCormick, D.A., 2000a. Cellular mechanisms of long-lasting adaptation in visual cortical neurons in vitro. J. Neurosci. 20, 4286–4299. https://doi.org/10.1523/jneurosci.20-11-04286.2000.

Sanchez-Vives, M.V., Nowak, L.G., McCormick, D.A., 2000b. Membrane mechanisms underlying contrast adaptation in cat area 17 in vivo. J. Neurosci. 20, 4267–4285. https://doi.org/10.1523/jneurosci.20-11-04267.2000.

Schwindt, P.C., Spain, W.J., Foehring, R.C., Stafstrom, C.E., Chubb, M.C., Crill, W.E., 1988. Multiple potassium conductances and their functions in neurons from cat sensorimotor cortex in vitro. J. Neurophysiol. 59, 424–449. https://doi.org/10.1152/jn.1988.59.2.424.

Sivaramakrishnan, S., Oliver, D.L., 2001. Distinct K currents result in physiologically distinct cell types in the inferior colliculus of the rat. J. Neurosci. 21, 2861–2877. https://doi.org/10.1523/JNEUROSCI.21-08-02861.2001.

Sun, H., Ma, C.L., Kelly, J.B., Wu, S.H., 2006. GABAB receptor-mediated presynaptic inhibition of glutamatergic transmission in the inferior colliculus. Neurosci. Lett. 399, 151–156. https://doi.org/10.1016/j.neulet.2006.01.049.

Tan, M.L., Theeuwes, H.P., Feenstra, L., Borst, J.G.G., 2007. Membrane properties and firing patterns of inferior colliculus neurons: an in vivo patch-clamp study in rodents. J. Neurophysiol. 98, 443–453. https://doi.org/10.1152/jn.01273.2006.

Ulanovsky, N., Las, L., Nelken, I., 2003. Processing of low-probability sounds by cortical neurons. Nat. Neurosci. 6, 391–398. https://doi.org/10.1038/nn1032.

Valdés-Baizabal, C., Parras, G.G., Ayala, Y.A., Malmierca, M.S., 2017. Endocannabinoid modulation of stimulus-specific adaptation in inferior colliculus neurons of the rat. Sci. Rep. 7, 1–14. https://doi.org/10.1038/s41598-017-07460-w.

Veenman, C.L., Reiner, A., Honig, M.G., 1992. Biotinylated dextran amine as an anterograde tracer for single- and double-labeling studies. J. Neurosci. Methods 41, 239–254.

Venkataraman, Y., Bartlett, E.L., 2013. Postnatal development of synaptic properties of the GABAergic projection from the inferior colliculus to the auditory thalamus. J. Neurophysiol. 109, 2866–2882. https://doi.org/10.1152/jn.00021.2013.

Wang, H., Han, Y.-F., Chan, Y.-S., He, J., 2014. Stimulus-specific adaptation at the synapse level in vitro. PloS One 9, e114537. https://doi.org/10.1371/journal.pone.0114537.

Wang, X.-J., Liu, Y., Sanchez-Vives, M.V., McCormick, D.A., 2003. Adaptation and temporal decorrelation by single neurons in the primary visual cortex. J. Neurophysiol. 89, 3279–3293. https://doi.org/10.1152/jn.00242.2003.

Wang, X.X., Jin, Y., Sun, H., Ma, C., Zhang, J., Wang, M., Chen, L., 2016. Characterization of rebound depolarization in neurons of the rat medial geniculate body in vitro. Neurosci. Bull. 32, 16–26. https://doi.org/10.1007/s12264-015-0006-5.

Wehr, M., Zador, A.M., 2005. Synaptic mechanisms of forward suppression in rat auditory cortex. Neuron 47, 437–445. https://doi.org/10.1016/j.neuron.2005.06.009.

Wu, S.H., Ma, C.L., Kelly, J.B., 2004. Contribution of AMPA, NMDA, and GABAA receptors to temporal pattern of postsynaptic responses in the inferior colliculus of the rat. J. Neurosci. 24, 4625–4634. https://doi.org/10.1523/JNEUROSCI.0318-04.2004.

Zhao, L., Liu, Y., Shen, L., Feng, L., Hong, B., 2011. Stimulus-specific adaptation and its dynamics in the inferior colliculus of rat. Neuroscience 181, 163–174. https://doi.org/10.1016/j.neuroscience.2011.01.060.

Please cite this article as: Valdés-Baizabal, C et al., *In vivo* whole-cell recordings of stimulus-specific adaptation in the inferior colliculus, Hearing Research, https://doi.org/10.1016/j.heares.2020.107978